Research Article Vol. 13, No. 2 / 1 Feb 2022 / Biomedical Optics Express 633
Biomedical Optics EXPRESS

Fluorescence lifetime needle optical biopsy discriminates hepatocellular carcinoma

EVGENII A. ZHEREBTSOV,[1,2,6,7] ELENA V. POTAPOVA,[1,6,8] ANDRIAN V. MAMOSHIN,[1,3] VALERY V. SHUPLETSOV,[1] KSENIA Y. KANDUROVA,[1] VIKTOR V. DREMIN,[1,4] ANDREY Y. ABRAMOV,[1,5] AND ANDREY V. DUNAEV[1]

[1]*Research & Development Center of Biomedical Photonics, Orel State University, Orel, Russia*
[2]*Optoelectronics and Measurement Techniques unit, University of Oulu, Oulu, Finland*
[3]*Orel Regional Clinical Hospital, Orel, Russia*
[4]*College of Engineering and Physical Sciences, Aston University, Birmingham, UK*
[5]*Department of Clinical and Movement Neurosciences, UCL Queen Square Institute of Neurology, London, UK*
[6]*Co-first authors with equal contribution*
[7]*evgenii.zherebtsov@oulu.fi*
[8]*e.potapova@oreluniver.ru*

Abstract: This work presents results of in vivo and in situ measurements of hepatocellular carcinoma by a developed optical biopsy system. Here, we describe the technical details of the implementation of fluorescence lifetime and diffuse reflectance measurements by the system, equipped with an original needle optical probe, compatible with the 17.5G biopsy needle standard. The fluorescence lifetime measurements observed by the setup were verified in fresh solutions of NADH and FAD^{++}, and then applied in a murine model for the characterisation of inoculated hepatocellular carcinoma (HCC) and adjacent liver tissue. The technique, applied in vivo and in situ and supplemented by measurements of blood oxygen saturation, made it possible to reveal statistically significant transformation in the set of measured parameters linked with the cellular pools of NADH and NADPH. In the animal model, we demonstrate that the characteristic changes in registered fluorescent parameters can be used to reliably distinguish the HCC tissue, liver tissue in the control, and the metabolically changed liver tissues of animals with the developed HCC tumour. For further transition to clinical applications, the optical biopsy system was tested during the routing procedure of the PNB in humans with suspected HCC. The comparison of the data from murine and human HCC tissues suggests that the tested animal model is generally representative in the sense of the registered fluorescence lifetime parameters, while statistically significant differences between their absolute values can still be observed.

1. Introduction

Primary and secondary cancer processes in the liver are among the most common causes of cancer death worldwide. At the moment, surgery is one of the main treatment methods for achieving the best results in the survival of patients with this pathology. Primary liver cancer includes hepatocellular carcinoma (HCC) (75–85% of cases) and cholangiocellular cancer (cholangiocarcinoma) (10–15% of cases), as well as other rare types [1]. The liver is the organ with the most frequent localisation of metastases of various cancer types: small and large intestines, lungs, pancreas, kidneys, breast, stomach, which is associated with the nature of blood circulation and liver function in the body. The prognosis of the disease strongly correlates with delayed diagnosis [2–4], so the key to successful treatment and recovery is early detection of the disease.

#447687 https://doi.org/10.1364/BOE.447687
Journal © 2022 Received 4 Nov 2021; revised 30 Nov 2021; accepted 30 Nov 2021; published 6 Jan 2022

Biomedical Optics EXPRESS

Surgeries performed at the first stages of liver cancer in many cases significantly reduce the risk of recurrence of the tumour [5]. According to modern medical views, the presence and nature of tumour pathology are verified only after histological and cytological analysis of the biopsy sample obtained with percutaneous needle biopsy (PNB), which remains the gold standard for the diagnosis of liver cancer [6]. However, the percentage of inadequate specimens when performing PNB can reach 10% [7].

When choosing a treatment strategy for patients with verified primary liver cancer, the surgeon relies on many factors. Evaluation of the prognosis of malignant tumours (in particular, primary liver tumours) is of particular relevance in determining further therapy. The prognosis for patients with liver cancer depends on several factors: tumour size, the number of foci and degree of malignancy, the patient's age, immune status and the severity of liver damage [8]. Morphological classification of tumours is clear, but it requires time and highly qualified specialists, so it is important to develop additional diagnostic methods that can differentiate between benign and malignant tumours directly during the examination and assess the degree of malignancy.

Optical technologies offer exceptional opportunities for accurate selection of the right areas for biopsy sampling, as they are highly sensitive to changes in the molecular and morphological structure of biological tissues. Moreover, these methods can be implemented as a fine-needle probe, which can provide information about tissue status in real-time during the standard PNB procedure.

One of the methods of optical biopsy widely used for monitoring cellular and tissue metabolism is fluorescence spectroscopy (FS) [9,10]. The use of endogenous fluorescence for the better diagnosis and treatment of malignant tumours has been demonstrated to be a useful instrument in both research and clinical studies. Several key components of living cells and tissues possess prominent endogenous fluorescence on illumination with light of UV or visible ranges [11–13]. The most abundant fluorescent cellular substances are NAD(P)H and FAD^{++} which are identified to be important participants in cell energy metabolism. As the malignant transformation is tightly linked with the crucial modification in energy metabolism, the co-factors can serve as biomarkers to distinguish normal and tumour tissues [14]. NADH and NADPH play different roles in a cell, as NADH is mostly involved in energy production, whereas NADPH is the key factor of glutathione recuperation for the purposes of antioxidant protection [15]. Both forms of NAD(P)H are indistinguishable from the position of their fluorescence spectra, but, being bound to proteins, their parameters of fluorescence lifetime change significantly. The use of fluorescence lifetime instruments has been proven to be a reliable method for characterisation of a cell based on its fluorescence lifetime parameters [16–18]. The shift in the energy-type production from oxidative phosphorylation to glycolysis and changes in the antioxidant defence of malignant cells can be effectively identified by their profile of the fluorescence lifetime of the NADH/NADPH components.

Currently, fine-needle probes for tumour diagnostics by the FS method during PNB have been developed for various organs. The research grade diagnostic accessories described in the literature are mostly based on assessing the changes in fluorescence intensity [19,20]. Earlier [21–23], we have demonstrated an optical biopsy system specially developed for *in vivo* tissue classification during the PNB of the liver. This system includes registration of the fluorescence intensity and diffuse reflectance spectra. In our and similar systems, the fluorescence intensity parameter allows us to evaluate the integral fluorescence of various tissue fluorophores [24]. Although we have shown that the shift of the fluorescence peak due to bile absorption can be successfully used for classification tasks, the parameter greatly depends on experimental conditions. These measurements are also affected by changes in probe contact with the tissue due to movements, non-uniform surface illumination, the presence of blood, and photobleaching. Such disturbing factors prevent the accurate direct assessment of redox ratio ($NADH/FAD^{++}$) from the intensity of fluorescence at the emission maxima of these substances.

Biomedical Optics EXPRESS

Techniques based on the registration of time-resolved FS are mostly free from these limitations. The measurement approach is sensitive to intermolecular interactions [25] and allows one to unmix endogenous fluorophores with overlapping spectra. That makes possible the separation of the total pool of NAD(P)H with different protein binding status by the analysis of the fluorescence components with short and long lifetimes. Changes in the free and bound NADH ratio are an effective tool to estimate the cellular metabolic redox status [26].

It should be noted that, due to technical problems of fast fluorescence decay measurements in the nanosecond range in the previous decade, a limited number of studies were published on the application of time-resolved FS for *in vivo* detection of tumour tissue and only the possibilities of their intraoperative use were shown. V. Sharma et al. showed the possibility of detecting invasive ductal breast carcinoma *ex vivo* using methods of time-resolved FS and DRS [27]. D. S. Kittle et al. described a time-resolved FS system designed to differentiate biological tissues based on their autofluorescence characteristics; it allowed them to differentiate tumour and normal tissues in real-time during surgical removal of a malignant brain tumour [28]. The research group led by Q. Fang developed a two-modal device that implements time-resolved FS and DRS methods, and presented ex vivo pilot clinical studies for detecting tumours of the brain [29], of the breast [30], and of the upper gastrointestinal tract [31]. For comparison with previously published data, here we present novel results of fluorescence lifetime (FSLT) measurements in hepatocellular carcinoma and healthy tissues of the liver obtained in a murine model and in the frame of limited clinical trials.

2. Methods and materials

2.1. Fluorescence lifetime optical biopsy system

The experimental setup combined two channels for the FSLT measurements and one channel for diffuse reflection spectra (DRS) recordings and calculation of the tissue oxygen saturation (Fig. 1). To measure the main FSLT parameters, we used the TCSPC system (Becker&Hickle, Germany) based on the SPC-130-EMN photon counting board and HPM-100-40 detectors and BDL-SMN 375 nm UV laser with FS emission detection in the range of 445 ± 25 nm. In the experimental work, one FSLT channel was employed with the MF445 filter. In the DRS channel, we used an HL-2000-FHSA tungsten halogen lamp (Ocean Insight, USA). Diffuse reflected radiation from tissue in the range of 400–900 nm was analysed using a Flame spectrometer (Ocean Insight, USA). In this study, both optical diagnostic technologies were incorporated by the use of the optical needle probe of 1 mm in diameter, compatible with the standard equipment for the puncture biopsy procedure, with the 17.5G Chiba-type biopsy needle [21]. For safety reasons, as well as to reduce the photobleaching effect, the radiation power of the 375 nm excitation source measured at the end of the optical needle probe did not exceed 0.2 mW. To calculate the safe level of radiation, we used the standards of the ICNIRP [34].

Since, in the experimental setup, a 375 nm UV laser was used, fluorescence from both cellular pools of NAD(P)H and FAD^{++} is expected to be excited. To simplify analysis in this work, we aimed at analysing only the NAD(P)H fluorescence. To verify that the setup reliably estimates the parameters of the FSLT and the used MF445 filter with the bandwidth of 445 ± 40 nm effectively blocks the emission of FAD^{++}, we recorded the fluorescence decay curves from fresh solutions of NADH and FAD^{++}, diluted in concentrations matching their possible concentrations in a living cell [36,37]. For the comparison, the filter MF479 with a transmission bandwidth of 479 ± 45 nm was used. Fig. 2 shows representative fluorescence decay traces measured in the 150 μM solutions of NADH and FAD^{++} with the 70 μW of UV laser power radiation on the tip of the probe using both filters (MF445 and MF479). The signal recorded from the FAD^{++} solution in the 445 ± 40 bandwidth was weak and mixed with background noise, so the accurate fitting procedure was hard to be implemented. The obtained data show that, when using a 445 nm filter, the signal from FAD^{++} solution is almost 20 times lower than the signal from NADH;

Biomedical Optics EXPRESS

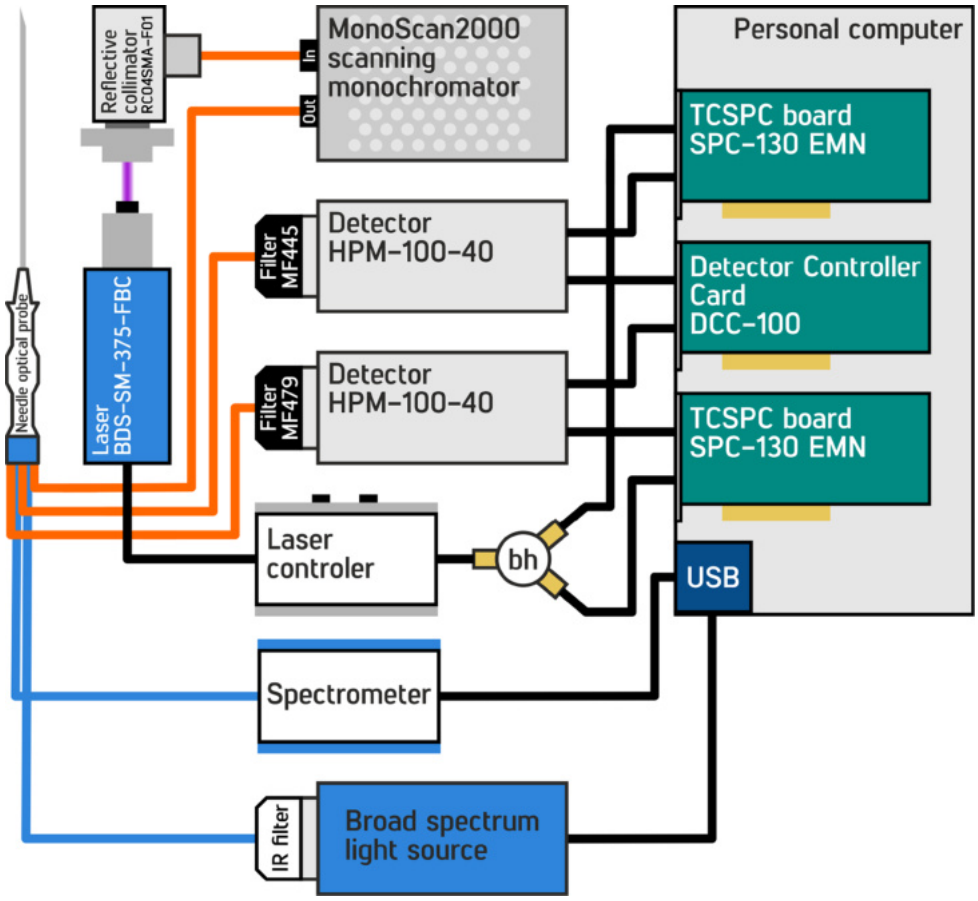

Fig. 1. Experimental setup comprising a channel for FSLT measurements and DRS recording for the estimation of the tissue oxygen saturation in the area of interest. Saturation was calculated using the previously developed approach based on a neural network fitting [21,32,33].

when using a 479 nm filter, the difference is reduced to less than 10 times. The measurements of NADH (with emission recorded in both 445 ± 40 nm and 479 ± 45 nm spectral regions) and FAD^{++} (with the emission measured in 479 ± 45 nm) processed by the one-exponential fitting model [35] allowed us to estimate corresponding lifetimes as follows: τ_{NADH} = 420 ± 10 ps and τ_{FAD} = 2350 ± 50 ps. The conducted preliminary tests and calibration allowed us to make an assumption that when we use a 445 nm filter to collect data, we mainly record the metabolic changes in the content of NAD(P)H.

2.2. Animal and prior clinical study

The hybrid BDF (C57Bl6xDBA) mice with inoculated tumours of the liver were provided by the N.N. Blokhin Russian Cancer Research Center (Moscow, Russia). For the murine model, H33 mouse HCC cells [38] (100 μl/mouse, 50000 cells/μl) were inoculated by injection of a suspension of cells into the right medial lobe of the liver of laboratory mice. Overall, six mice at the end-stage of HCC tumour development and four healthy control animals took part in the procedure. Measurements were taken no earlier than three months after inoculation. The end-stages of liver cancer were determined during dynamic observation of the animals by the

Biomedical Optics EXPRESS

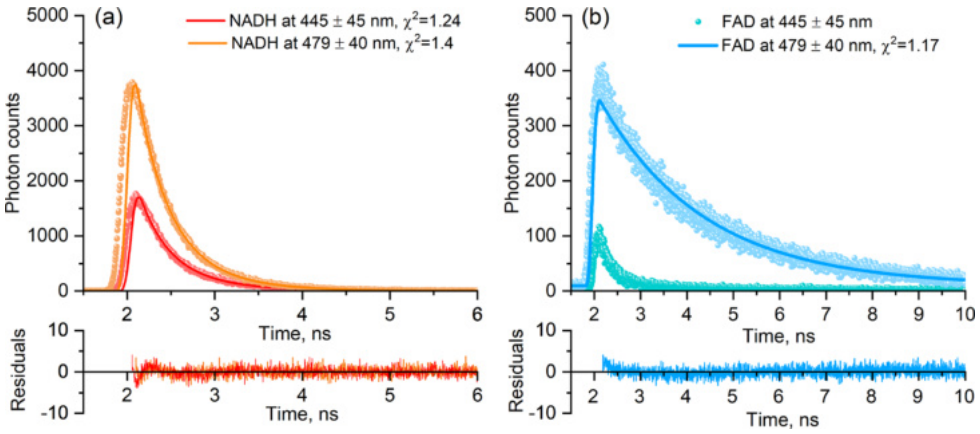

Fig. 2. Relevant traces of fluorescence decay recorded by the setup through the needle optical probe from the buffer solutions of NADH and FAD^{++} with $\tau_{NADH} = 420 \pm 10$ ps and $\tau_{FAD} = 2350 \pm 50$ ps reconstructed by the one-exponentional fitting model [35]. a) FAD – emission detection in the range of 445 ± 25 nm, b) FAD^{++} – emission detection in the range of 479 ± 40 nm, c) NADH – emission detection in the range of 445 ± 25 nm, d) NADH – emission detection in the range of 479 ± 40 nm.

combination of the following parameters: changes in body weight, abdominal circumference, the appearance of ascites, muscle tension of the anterior abdominal wall, the presence of tumour-like formation on palpation, decreased appetite and motor activity in mice.

The animal study was approved by the local Ethics committee of Orel State University (record of the meeting No. 12 of 06.09.2018) in accordance with GLP principles. During the study, mice were anesthetized with Zoletil 100, at standard dosages. Each animal was fixed on a special platform in the position on its back. Then a laparotomy, *in vivo* experimental measurements by the optical needle probe and standard biopsy sampling procedure of the liver tumour were performed (Fig. 3).

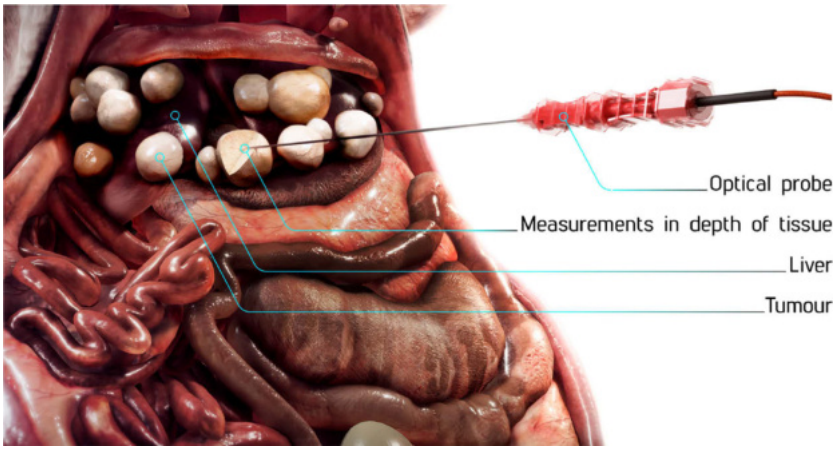

Fig. 3. The measurements have been conducted through the needle optical probe on the H33 HCC inoculated to liver in the murine model.

At this stage of our research, preliminary measurements were made at the department of interventional radiology of Orel Regional Clinical Hospital (Orel, Russia). The study was

Biomedical Optics EXPRESS

approved by the Ethics committee of Orel State University (record of the meeting No. 14 of 24.01.2019) and carried out in accordance with the 2013 Declaration of Helsinki by the World Medical Association. The measurements in the murine model and in patients with HCC were supported and confirmed by histological analysis.

2.3. Statistical analysis

Taking into account the limited sample sizes, the non-parametric Mann-Whitney U-test was chosen to validate the reliability of statistical differences in the results. A linear discriminant analysis (LDA) was used to determine the discriminant function. To ensure the stability of the classifier and avoid over-fitting, leave-one-out cross-validation was used. n-1 observations of the dataset were used to train LDA and the remaining one observation was used to predict the response value. This process was repeated until each of the observations was used for testing and, in the end, the averaged model accuracy from all iterations was reported.

3. Results and discussion

Measurements of the tissue oxygen saturation (StO_2) in the developed lumps of the HCC tumour, adjacent regions of liver tissue and liver tissue in healthy control animals showed that they do not have equal StO_2. The highest values of StO_2 were observed in the tested points of the HCC tumour (84.6±0.1%, $p<0.001$, Fig. 4(a). The parameter in the adjacent liver tissue was also higher compared to the values in the control liver tissue (83.0±0.1% and 80.9±0.1% correspondingly, $p<0.001$, Fig. 4(a). As in the studies that we have previously published [21], a statistically significant difference in the oxygen saturation of two types of tissues was detected. The oxygen saturation of HCC tissues is higher than in liver tissue in the metabolically changed liver tissues of animals with the developed HCC tumour. The most likely explanation of this is the difference in their blood supply. The liver is unique in that it gets a double perfusion from both arterial and venous blood, a portal component of blood supplies of 75 to 80% and an arterial component of approximately 20 to 25%. During the development of the HCC, perfusion from the aberrant arterioles gradually replaces the normal double perfusion from the paired vessels [39,40]. This has been confirmed in some mouse models of HCC [41].

The fluorescence intensity I_f measured in the HCC tumour lumps was significantly higher (more than two times) than in the liver tissues of the control animals, which were free of tumour cells ($2.30 \cdot 10^6 \pm 0.1 \cdot 10^6$ photons and $0.9 \cdot 10^6 \pm 0.03 \cdot 10^6$ photons correspondingly, $p<0.001$, Fig. 4(b). Interestingly, the level of fluorescence intensity in the liver tissues adjacent to the areas of HCC ($2.07 \cdot 10^6 \pm 0.1 \cdot 10^6$ photons) was not significantly different from the values measured in the tumour ($p>0.1$). This fact brings into question the use the fluorescence intensity as a single parameter to distinguish end-stage tumours associated with HCC and adjacent liver tissues.

The increase in the NAD(P)H might be an explanation, but this interpretation should rather be rejected, as the higher levels of fluorescence intensity are not accompanied by a decrease in the short lifetime τ_1. The amplitude of the short decay component (α_1) was significantly higher in the *in vivo* characterised HCC tumour lumps in comparison with the adjacent areas of the liver tissue of the same animal, as well as when compared with the liver tissues of control animals (4600 ± 260 photons, 1840 ± 100 photons and 1107 ± 48 photons correspondingly, $p<0.001$, Fig. 4(c). Similarly to the total fluorescence intensity, the amplitude also differed for the liver tissue measurements in animals with HCC and control group, but the level of statistical significance was lower ($p<0.01$, Fig. 4(b).

The amplitude of the long decay component (α_2) was also highest in the HCC lumps, while this parameter demonstrated the lowest level in the liver of the control group (1430 ± 75 photons and 680 ± 27 photons correspondingly, $p<0.001$, Fig. 4(d). The liver tissues adjacent to the tumour had intermediate level of α_2 (1080 ± 60 photons) allocated between the parameter levels in the tumour and in the control, with a statistically significant difference when compared with

Biomedical Optics EXPRESS

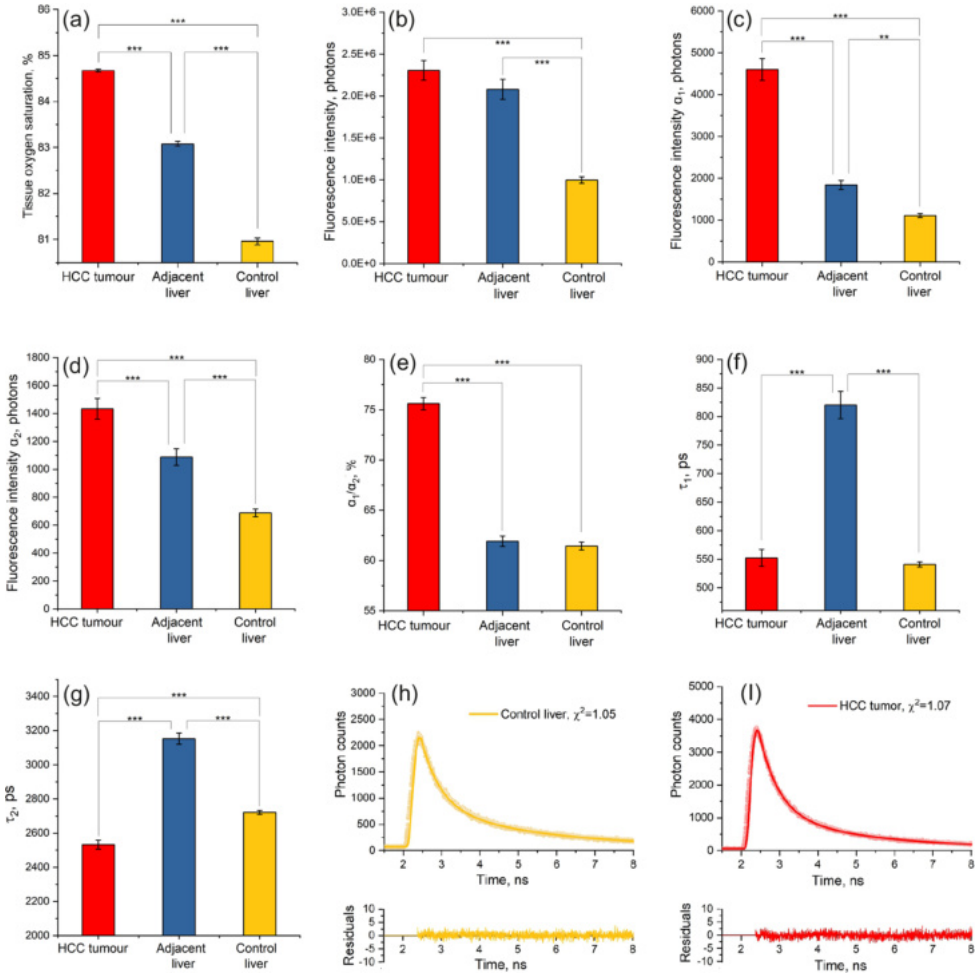

Fig. 4. Parameters evaluated by the fluorescence lifetime measurements through the needle optical probe in the murine model with the inoculated HCC and in the control group of animals. a) tissue oxygen saturation evaluated by diffuse reflectance spectroscopy; b) total fluorescence intensity; c) the amplitude of the short decay component, α_1; d) the amplitude of the long decay component, α_2; e) amplitude ratio, α_1/α_2; f) short fluorescence lifetime, τ_1;g) long fluorescence lifetime, τ_2; h) a biexponential decay model adequately described the NAD(P)H fluorescence decay measured in the liver tissues of control animals; i) a biexponential decay model adequately described the NAD(P)H fluorescence decay measured in the tumour. A single SE was taken to plot error bars.

each of them (p<0.001). The combined data for both α_1 and α_2 assumes that the main reason for the increased fluorescence intensity in adjacent liver tissue is emission from molecules having the longer fluorescence lifetime, such as protein-bound NADH.

Despite the difference in absolute values of the α_1 and α_2, the amplitude ratio, α_1/α_2 demonstrated no significant difference between the two characterised cases of the liver tissue. The ratio α_1/α_2 measured in HCC lumps was significantly higher when compared with both the adjacent liver tissue of the same animal and the liver tissues of control animals (75.6 ± 0.6%, 61.9 ± 0.5% and 61.4 ± 0.4% correspondingly, p<0.001, Fig. 4(e). No significant difference was highlighted between the HCC tumour and the liver tissue of control animals as far as the parameter

Biomedical Optics EXPRESS

of short fluorescence lifetime, τ_1 is concerned (552 ± 15 ps and 540 ± 5 ps correspondingly, $p>0.1$, Fig. 4(f). In contrast, the values of τ_1 in liver tissues surrounding the tumour significantly exceeded both the values measured in the tumour lumps and in the liver tissue of control animals (820 ± 24 ps, $p<0.001$). For the measured parameters of long fluorescence lifetime (τ_2), we obtained similar results with the increased lifetime for the liver tissues adjacent to the tumour (3150 ± 30 ps, $p<0.001$, Fig. 4(g) except the parameter was significantly lower for the HCC tumour when compared with the liver of the controls (2530 ± 25 ps and 2720 ± 10 ps correspondingly, $p<0.001$).

The measured value of τ_2 was higher than the values of this parameter for pure NADH. Previously the lifetimes corresponding to protein-bound NADH were determined to be 3120.7 ± 291.8 ps in normal liver and 2541.7 ±341.8 ps in liver with hepatocellular carcinoma [42]. These results are close to what we observed. The decrease of τ_2 is a known effect associated with the metabolic shift in cancer cells and expressed in the increase of the free NADH and the potential decrease of the protein-bound fraction of NADH [43,44]. It may also be connected with a change in the intensity of antioxidant defense [45,46].

The blood oxygen saturation has a direct impact on the mitochondrial energy production, and the content of NADH as a major player substance in the processes of glycolysis and oxidative phosphorylation. Despite the importance of understanding the interplay of the tissue oxygen supply and the registering parameters of the endogenous fluorescence for the *in vivo* fluorescence diagnostics, few researchers have addressed the question with an approach beyond studies with single cells.

The obtained data demonstrate that fluorescence intensity cannot be accepted alone as a reliable marker to distinguish HCC from non-cancerous liver tissue. This claim is essentially relevant for the task of the precise navigation of the PNB tool to nullify the probability of non-diagnostic biopsy samples from patients with the presence of liver cancer suspected but not yet discovered. The statistics obtained on the values shown in Fig. 4 imply that the calculated parameters of the fluorescence decay curve may provide a better alternative to diagnostics based only on measurements of fluorescence intensity. Apparently, the parameters of promising interest are the short and long fluorescence lifetimes (τ_1, τ_2) and the amplitude ratio α_1/α_2. A diagnostic classifier can be implemented, not only based on a single parameter, but with a vector of input coefficients weakly correlated with each other. Thus, the set of mutually independent parameters which can be obtained with the TCSPC system with a model of two-exponential decay of fluorescence is as follows: τ_1, τ_2, α_1/α_2 and fluorescence intensity I_f.

The measured data and the multi-exponential model for liver tissues of control animals and tumours are shown in Fig. 4(h) and (i) respectively.

To assess the diagnostic value of the feature space to distinguish the HCC and liver tissues, we have applied the formalism of linear discriminant analysis (LDA). This method demonstrates acceptable performance when applied to limited training sets. It is known that the sample size applies a limit to the optimal dimension of the input feature vector [47]. Taking into account the number of measured samples, for this study we analysed the LDA classifiers built on the pairs of the independent parameters (τ_1, α_1/α_2), (τ_2, α_1/α_2), (τ_1, I_f) and (τ_2, I_f). Fig. 5 demonstrates the distribution of the obtained data points in the coordinate spaces of the (τ_1, I_f) and (τ_2, I_f) parameter pairs. The delineation of the classes of HCC tissues and the normal liver tissue of the control animals with the use of the input fluorescence parameters is shown in Fig. 5(a,b). The separation of the classes of HCC tumour areas and adjacent liver tissue of the animals where the tumour developed is shown in Fig. 5(c,d).

Fig. 6 shows the allocation of the data points in the coordinate space of the (τ_1, α_1/α_2) and (τ_2, α_1/α_2) parameters, where the parameter I_f was replaced with the ratio of α_1/α_2. To figure out the LDA parameters, the data measured in the studied animals were used. In addition, to every plot, we have added the data points measured during the PNB procedure in patients with

Biomedical Optics EXPRESS

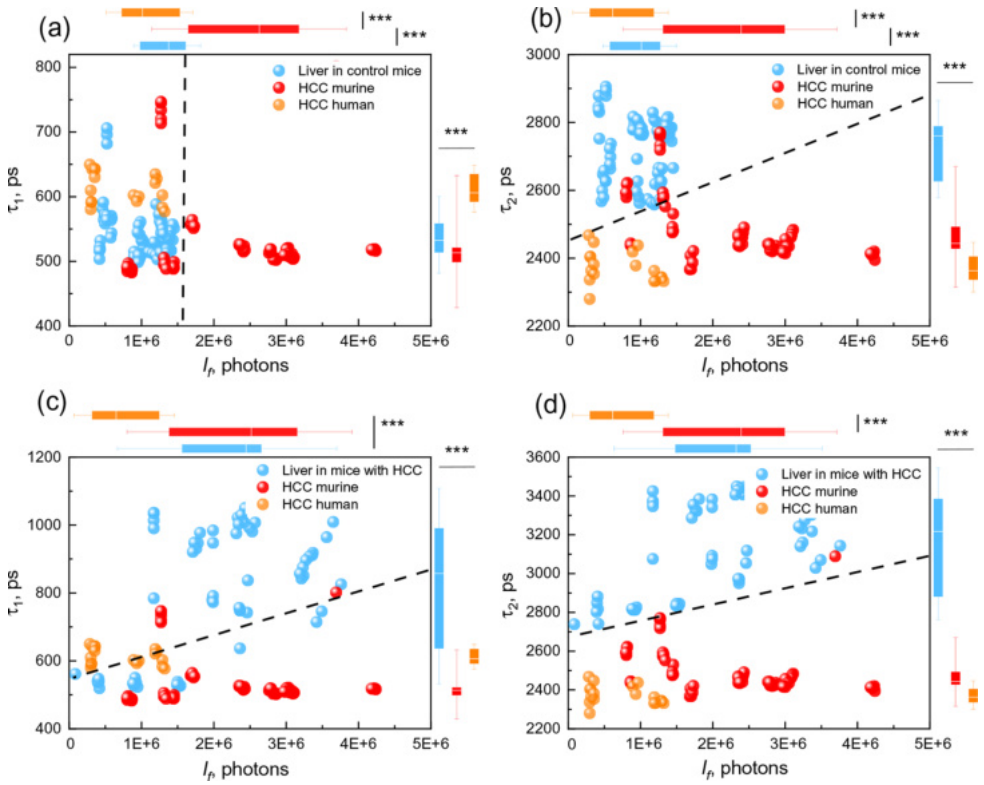

Fig. 5. The LDA classification based on the parameters of lifetime (τ_1 and τ_2) and fluorescence intensity I_f. (a) and (b) Decision boundary lines for the separation of murine HCC and liver tissues in control mice in the coordinate spaces of (τ_1, I_f) and (τ_2, I_f). (c), (d) Decision boundary lines obtained using the same pairs of parameters for the separation of the data points from murine HCC and liver tissues in the mice with tumours. Statistical significance is determined by Mann-Whitney U-test, $p<0.001$; error bars are equal to 1.5 SD.

retrospectively confirmed primary HCC. The data measured in humans were not used for the calculation of the discriminant functions, but were compared with the data measured in the murine model. The candlestick charts placed on the top and on the right sides of the scattering plots in Fig. 5 and Fig. 6 indicate the presence of the statistically confirmed difference between the coordinates of the data points (by Mann-Whitney U-test, $p<0.001$; 1.5 SD is taken to plot error bars). The data from murine and human HCC tissues suggests that the tested animal model is representative in general in the sense of the registered fluorescence lifetime parameters when compared with the values of the parameters measured in liver tissue. Nevertheless, statistically significant differences between murine and human HCC were observed in all parameters. The values of the coefficients for the separating lines from Fig. 6 and Fig. 5 are given in Table 1. The estimated parameters of sensitivity, specificity and AUC for the achieved discrimination of HCC from liver tissue in control animals and mice with end-stage HCC development are presented in Table 2.

The parameters of registered fluorescence intensity I_f demonstrate the poorest diagnostic significance for both compared classes of murine liver with the HCC tumour. The predictive value of the τ_1 parameters is not equal between the cases of distinguishing HCC H33 tumours from liver tissues in control and ones in the mice with the inoculated HCC H33. In the case of the separating pair "murine HCC - control animals", the τ_1 does not demonstrate a tangible

Biomedical Optics EXPRESS

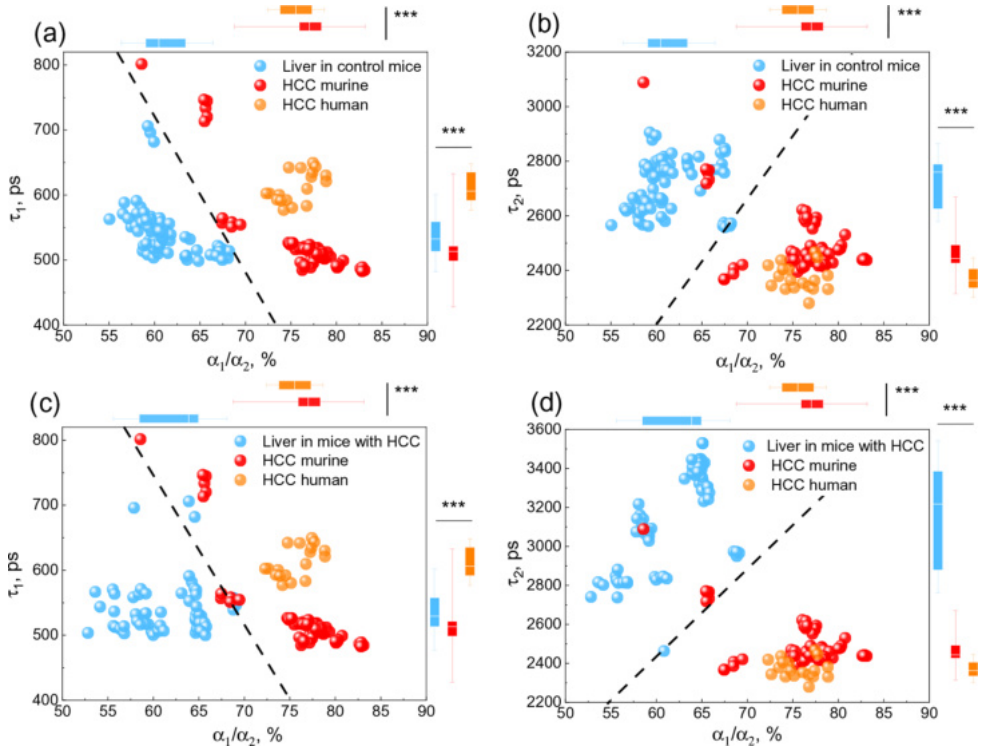

Fig. 6. The LDA classification based on the parameters of lifetime (τ_1 and τ_2) and ratio α_1/α_2. (a), (b) Decision boundary lines for the separation of murine HCC and liver tissues in control mice in the coordinate spaces of the (τ_1, α_1/α_2) and (τ_2, α_1/α_2). (c), (d) Decision boundary lines obtained using the same pairs of parameters for the separation of the data points from murine HCC and liver tissues in the mice with tumours. Statistical significance is determined by Mann-Whitney U-test, $p<0.001$; error bars are equal to 1.5 SD.

Table 1. The obtained parameters of the linear discriminant functions in the form of $k_1X_1 + k_2X_2 + C = 0$ for the separation of the data points for HCC and liver tissue in control animals and mice with end-stage HCC development

Parameters	Control liver - murine HCC			Adjacent liver - murine HCC		
	k_1	k_2	C	k_1	k_2	C
$\tau_1, \alpha_1/\alpha_2$	1.06	0.05	-96.79	1.02	0.04	-93.59
$\tau_2, \alpha_1/\alpha_2$	0.65	-0.01	-8.83	0.87	-0.02	-2.54
τ_1, I_f	$2.35 \cdot 10^{-6}$	$-2.8 \cdot 10^{-4}$	-3.71	$1.03 \cdot 10^{-6}$	$-1.69 \cdot 10^{-2}$	9.26
τ_2, I_f	$1.72 \cdot 10^{-6}$	$-1.70 \cdot 10^{-2}$	41.39	$9.58 \cdot 10^{-7}$	$-1.76 \cdot 10^{-2}$	47.81

Table 2. The obtained parameters of sensitivity, specificity and AUC for the discrimination of HCC from liver tissue in control animals and mice with end-stage HCC development

Parameters	Control liver - murine HCC			Adjacent liver - murine HCC		
	Sensitivity	Specificity	AUC	Sensitivity	Specificity	AUC
$\tau_1, \alpha_1/\alpha_2$	0.9	1.0	0.98	0.65	1.0	0.99
$\tau_2, \alpha_1/\alpha_2$	0.87	0.97	0.97	0.79	0.96	0.99
τ_1, I_f	0.97	0.91	0.86	0.92	0.72	0.96
τ_2, I_f	0.92	0.99	0.94	0.99	0.99	0.99

Biomedical Optics EXPRESS

importance, while the elevated values of the parameters in the liver of animals with HCC tumour allow this measurement to contribute to the total quality of the classification for the pair "murine HCC - adjacent liver tissue". As a result, the LDA classifiers in the (τ_1, I_f) coordinate space show the worst quality indicators, with the AUC estimated as 0.86 and 0.96 for the first and second pairs of classes, respectively. In contrast, the τ_2 and α_1/α_2 parameters were identified to be of the highest diagnostic significance in the considered task of HCC tumour discovery. The delineation with the use of the (τ_2, α_1/α_2) input vector demonstrated highly robust results, with the AUC values as 0.97 and 0.99. The two analysed parameters, when combined with the τ_2 or I_f, can also be used to achieve significant levels of classification quality. The AUC parameter for the input vector (τ_2, I_f) in the analysed classes was estimated as 0.94 and 0.99. For the (τ_1, α_1/α_2), the AUC was 0.98 and 0.99, respectively.

Although a preliminary diagnosis of primary liver cancer (HCC) is usually made on the basis of imaging techniques (CT, ultrasound, MRI) and measurements of oncofetal antigens (especially α-fetoprotein), there is currently no single technology that can replicate all the advantages of biopsy [48]. Liver biopsy remains the gold standard for diagnosing liver neoplasms and for measuring inflammation, fibrosis, and degree of steatosis [49]. Radiological imaging does not always allow precise characterisation of the tumour, especially in small HCCs (<2 cm) [50]. A liver biopsy, like all other medical instruments, has its limitations. Standard biopsy procedures can miss small tumour lesions due to location, size and respiratory motion during the biopsy procedure. Accurate real-time tissue identification during biopsy procedures can significantly improve the diagnostic biopsy procedure by providing accurate tissue sampling from tumours for further histological analysis. This can help to increase the number of adequate biopsy samples for histopathological analysis.

This work shows that the use of reference data measured in healthy liver tissue can be a source of serious inaccuracy when applied to distinguish the tissues of tumour and adjacent liver. The results obtained demonstrate that the cancerous processes in surrounding liver tissues may significantly alter the metabolic state in the liver cells, which manifests itself in the modified set of observed fluorescence lifetime parameters. The uncertainty around the actual level of the liver disease in a patient undergoing PNB procedure, when gradual transition of the liver tissue from the healthy state to prominent degrees of pathology can take place, should be considered. In that respect, the proposed (τ_2, α_1/α_2) vector of input parameters may have a sufficient level of robustness to the factor of uncertainty.

The research protocol of the conducted preliminary clinical studies was not designed to assess the stage of the fluorescence measurements in the liver tissue of the patients; nevertheless, this aspect of characterisation is admitted to be crucial for the successful transition of the developing technology to the level of widely adopted clinical routine procedure. The next steps of the development will be taken towards the identification of benign tumours, as well as collecting a relevant dataset of the fluorescence lifetime parameters from the most frequent metastases that occur in the liver (such as adenocarcinoma metastasis of different origins).

4. Conclusion

In this paper, we present the technical details of the developed optical biopsy system, which implements FSLT and DRS measurements. The technology was verified on laboratory mice with inoculated murine HCC H33, as well as in a preliminary clinical study in patients with suspected, and subsequently confirmed, primary liver cancer – HCC. We demonstrate that the registered set of independent diagnostic parameters being applied, together with even a basic classification algorithm, allows us to reliably distinguish HCC tissue, healthy liver tissue and the metabolically changed liver tissues around the developed HCC tumour. Analysis of the obtained results shows the high sensitivity and specificity of the proposed optical biopsy technique, benefiting from the on-the-site characterisation of the tissue on the tip of the optical needle probe before the

Biomedical Optics EXPRESS

sample is taken. The study lays the groundwork for further industrialised implementation of the fluorescence lifetime needle optical biopsy with real-time retrieval of the diagnostic parameters, and decision-making based on more advanced machine learning techniques.

Funding. Russian Science Foundation (21-15-00325); Russian Federation Government (075-15-2019-1877); Academy of Finland (318281).

Acknowledgements. The authors acknowledge the support of the Russian Science Foundation under project No. 21-15-00325 (development of an optical biopsy system and conducting experimental study) and the Russian Federation Government grant No. 075-15-2019-1877 (separation and analysis of free NADH and the protein-bound fraction of NADH), grant Academy of Finland No. 318281 (data visualisation). The authors are very grateful to Dr. Olga V. Morozova (N.N. Blokhin Russian Cancer Research Center, Moscow, Russia) for tumour cell inoculation.

Disclosures. The authors declare no conflicts of interest.

Data availability. Data underlying the results may be obtained from the authors upon reasonable request.

References

1. F. Bray, J. Ferlay, I. Soerjomataram, R. L. Siegel, L. A. Torre, and A. Jemal, "Global cancer statistics 2018: Globocan estimates of incidence and mortality worldwide for 36 cancers in 185 countries," CA: A Cancer Journal for Clinicians **68**, 394–424 (2018).
2. J. Bruix, M. Reig, and M. Sherman, "Evidence-based diagnosis, staging, and treatment of patients with hepatocellular carcinoma," Gastroenterology **150**, 835–853 (2016).
3. M. H. Attwa and S. A. El-Etreby, "Guide for diagnosis and treatment of hepatocellular carcinoma," WJH **7**, 1632 (2015).
4. C. Stavraka, H. Rush, and P. Ross, "Combined hepatocellular cholangiocarcinoma (cHCC-CC): an update of genetics, molecular biology, and therapeutic interventions," J. Hepatocell. Carcinoma **6**, 11–21 (2019).
5. S. Roayaie, K. Obeidat, C. Sposito, L. Mariani, S. Bhoori, A. Pellegrinelli, D. Labow, J. M. Llovet, M. Schwartz, and V. Mazzaferro, "Resection of hepatocellular cancer <= 2 cm: Results from two Western centers," Hepatology **57**, 1426–1435 (2013).
6. D. C. Rockey, S. H. Caldwell, Z. D. Goodman, R. C. Nelson, and A. D. Smith, "Liver biopsy," Hepatology **49**, 1017–1044 (2009).
7. S.-M. Park, D.-W. Lee, S.-Y. Jin, D.-W. Kim, Y.-M. Jeen, and I.-H. Choi, "Fine-needle aspiration cytology as the first pathological diagnostic modality in breast lesions: A comparison with core needle biopsy," Basic Appl. Pathol. **3**, 18 (2010).
8. A. Forner, M. Reig, and J. Bruix, "Hepatocellular carcinoma," The Lancet **391**, 1301–1314 (2018).
9. M. Y. Berezin and S. Achilefu, "Fluorescence lifetime measurements and biological imaging," Chem. Rev. **110**, 2641–2684 (2010).
10. N. Ramanujam, "Fluorescence spectroscopy of neoplastic and non-neoplastic tissues," Neoplasia **2**, 89–117 (2000).
11. F. Bartolomé and A. Y. Abramov, "Measurement of mitochondrial NADH and FAD autofluorescence in live cells," Methods in Molecular Biology **1264**, 263–270 (2015).
12. A. Y. Vinokurov, V. V. Dremin, G. A. Piavchenko, O. A. Stelmashchuk, P. R. Angelova, and A. Y. Abramov, "Assessment of mitochondrial membrane potential and NADH redox state in acute brain slices," Methods in Molecular Biology **2276**, 193–202 (2021).
13. A. C. Croce and G. Bottiroli, "Autofluorescence spectroscopy and imaging: a tool for biomedical research and diagnosis," Eur. J. Histochem. **58**, 2461 (2014).
14. K. Awasthi, D. Moriya, T. Nakabayashi, L. Li, and N. Ohta, "Sensitive detection of intracellular environment of normal and cancer cells by autofluorescence lifetime imaging," Journal of Photochemistry and Photobiology B: Biology **165**, 256–265 (2016).
15. H.-Q. Ju, J.-F. Lin, T. Tian, D. Xie, and R.-H. Xu, "Nadph homeostasis in cancer: functions, mechanisms and therapeutic implications," Sig Transduct Target Ther **5**, 231 (2020).
16. W. Becker, A. Bergmann, M. Hink, K. König, K. Benndorf, and C. Biskup, "Fluorescence lifetime imaging by time-correlated single-photon counting," Microsc. Res. Tech. **63**, 58–66 (2004).
17. L. Marcu, "Fluorescence lifetime images and correlation spectra obtained by multidimensional time-correlated single photon counting," Ann. Biomed. Eng. **40**, 304–331 (2012).
18. R. Datta, T. M. Heaster, J. T. Sharick, A. A. Gillette, and M. C. Skala, "Fluorescence lifetime imaging microscopy: fundamentals and advances in instrumentation, analysis, and applications," J. Biomed. Opt. **25**, 71203 (2020).
19. M.-C. Mathieu, A. Toullec, C. Benoit, R. Berry, P. Validire, P. Beaumel, Y. Vincent, P. Maroun, P. Vielh, L. Alchab, R. Farcy, H. Moniz-Koum, M.-P. Fontaine-Aupart, S. Delaloge, and C. Balleyguier, "Preclinical *ex vivo* evaluation of the diagnostic performance of a new device for *in situ* label-free fluorescence spectral analysis of breast masses," Eur Radiol **28**, 2507–2515 (2018).
20. E. Tanis, D. J. Evers, J. W. Spliethoff, V. V. Pully, K. Kuhlmann, F. van Coevorden, B. H. Hendriks, J. Sanders, W. Prevoo, and T. J. Ruers, "*In vivo* tumor identification of colorectal liver metastases with diffuse reflectance and fluorescence spectroscopy," Lasers Surg. Med. **48**, 820–827 (2016).

Biomedical Optics EXPRESS

21. V. Dremin, E. Potapova, E. Zherebtsov, K. Kandurova, V. Shupletsov, A. Alekseyev, A. Mamoshin, and A. Dunaev, "Optical percutaneous needle biopsy of the liver: a pilot animal and clinical study," Sci. Rep. **10**, 14200 (2020).
22. K. Y. Kandurova, E. V. Potapova, E. A. Zherebtsov, V. V. Dremin, E. S. Seryogina, A. Y. Vinokurov, A. V. Mamoshin, A. V. Borsukov, Y. V. Ivanov, and A. V. Dunaev, "Testing a fine-needle optical probe for recording changes in the fluorescence of coenzymes of cellular respiration," Opt. Spectrosc. **128**, 742–751 (2020).
23. V. Dremin, E. Potapova, E. Zherebtsov, I. Kozlov, E. Seryogina, K. Kandurova, A. Alekseyev, G. Piavchenko, S. Kuznetsov, A. Mamoshin, and A. Dunaev, "Optical fine-needle aspiration biopsy in a rat model," Proc. SPIE **10877**, 108770K (2019).
24. E. Zherebtsov, M. Zajnulina, K. Kandurova, E. Potapova, V. Dremin, S. Mamoshin, A. Dunaev, and E. U. Rafailov, "Machine learning aided photonic diagnostic system for minimally invasive optically guided surgery in the hepatoduodenal area," Diagnostics **10**, 873 (2020).
25. K. Suhling, P. M. French, and D. Phillips, "Time-resolved fluorescence microscopy," Photochem. Photobiol. Sci. **4**, 13–22 (2005).
26. M. C. Skala, K. M. Riching, D. K. Bird, A. Gendron-Fitzpatrick, J. Eickhoff, K. W. Eliceiri, P. J. Keely, and N. Ramanujam, "*In vivo* multiphoton fluorescence lifetime imaging of protein-bound and free nicotinamide adenine dinucleotide in normal and precancerous epithelia," J. Biomed. Opt. **12**, 024014 (2007).
27. V. Sharma, S. Shivalingaiah, Y. Peng, D. Euhus, Z. Gryczynski, and H. Liu, "Auto-fluorescence lifetime and light reflectance spectroscopy for breast cancer diagnosis: potential tools for intraoperative margin detection," Biomed. Opt. Express **3**, 1825–1840 (2012).
28. D. S. Kittle, F. Vasefi, C. G. Patil, A. Mamelak, K. L. Black, and P. V. Butte, "Real time optical biopsy: time-resolved fluorescence spectroscopy instrumentation and validation," Sci. Rep **6**, 38190 (2016).
29. Z. Nie, V. N. Du Le, D. Cappon, J. Provias, N. Murty, J. E. Hayward, T. J. Farrell, M. S. Patterson, W. McMillan, and Q. Fang, "Integrated time-resolved fluorescence and diffuse reflectance spectroscopy instrument for intraoperative detection of brain tumor margin," IEEE J. Sel. Top. Quantum Electron. **22**, 49–57 (2015).
30. N. Shalaby, A. Al-Ebraheem, D. Le, S. Cornacchi, Q. Fang, T. Farrell, P. Lovrics, G. Gohla, S. Reid, N. Hodgson, and F. Michael, "Time-resolved fluorescence and diffuse reflectance spectroscopy for margin analysis in breast cancer," Lasers Surg. Med. **50**, 236–245 (2018).
31. Z. Nie, S.-C. A. Yeh, M. LePalud, F. Badr, F. Tse, D. Armstrong, L. W. Liu, M. J. Deen, and Q. Fang, "Optical biopsy of the upper gi tract using fluorescence lifetime and spectra," Front. Physiol. **11**, 339 (2020).
32. E. Zherebtsov, V. Dremin, A. Popov, A. Doronin, D. Kurakina, M. Kirillin, I. Meglinski, and A. Bykov, "Hyperspectral imaging of human skin aided by artificial neural networks," Biomed. Opt. Express **10**, 3545 (2019).
33. V. Dremin, Z. Marcinkevics, E. Zherebtsov, A. Popov, A. Grabovskis, H. Kronberga, K. Geldnere, A. Doronin, I. Meglinski, and A. Bykov, "Skin complications of diabetes mellitus revealed by polarized hyperspectral imaging and machine learning," IEEE Trans. Med. Imaging **40**, 1207–1216 (2021).
34. I. C. on Non-Ionizing Radiation Protection, "Guidelines on limits of exposure to ultraviolet radiation of wavelengths between 180 nm and 400 nm (incoherent optical radiation)," Health Phys. **87**, 171–186 (2004).
35. R. Cao, H. K. Wallrabe, and A. Periasamy, "Multiphoton FLIM imaging of NAD(P)H and FAD with one excitation wavelength," J. Biomed. Opt. **25**, 014510 (2020).
36. N. Ma, M. A. Digman, L. Malacrida, and E. Gratton, "Measurements of absolute concentrations of NADH in cells using the phasor FLIM method," Biomed. Opt. Express **7**, 2441 (2016).
37. A. A. Heikal, "Intracellular coenzymes as natural biomarkers for metabolic activities and mitochondrial anomalies," Biomarkers in medicine **4**, 241 (2010).
38. N. L. Lazarevich, O. A. Cheremnova, E. V. Varga, D. A. Ovchinnikov, E. I. Kudrjavtseva, O. V. Morozova, D. I. Fleishman, N. V. Engelhardt, and S. A. Duncan, "Progression of hcc in mice is associated with a downregulation in the expression of hepatocyte nuclear factors," Hepatology **39**, 1038–1047 (2004).
39. J.-A. Chen, M. Shi, J.-Q. Li, and C.-N. Qian, "Angiogenesis: multiple masks in hepatocellular carcinoma and liver regeneration," Hepatol. Int. **4**, 537–547 (2010).
40. J. Cazejust, B. Bessoud, N. Colignon, C. Garcia-Alba, O. Planché, and Y. Menu, "Hepatocellular carcinoma vascularization: from the most common to the lesser known arteries," Diagnostic and Interventional Imaging **95**, 27–36 (2014).
41. S. K. Kim, H. Kim, G. Y. Koh, D.-S. Lim, D.-Y. Yu, M. D. Kim, M.-S. Park, and J. S. Lim, "Mouse hepatic tumor vascular imaging by experimental selective angiography," PLoS One **10**, e0131687 (2015).
42. H. Wang, X. Liang, Y. H. Mohammed, J. A. Thomas, K. R. Bridle, C. A. Thorling, J. E. Grice, Z. P. Xu, X. Liu, D. H. Crawford, and M. S. Roberts, "Real-time histology in liver disease using multiphoton microscopy with fluorescence lifetime imaging," Biomed. Opt. Express **6**, 780–792 (2015).
43. T. S. Blacker, Z. F. Mann, J. E. Gale, M. Ziegler, A. J. Bain, G. Szabadkai, and M. R. Duchen, "Separating NADH and NADPH fluorescence in live cells and tissues using FLIM," Nat. Commun. **5**, 3936 (2014).
44. S. Rodimova, D. Kuznetsova, N. Bobrov, V. Elagin, V. Shcheslavskiy, V. Zagainov, and E. Zagaynova, "Mapping metabolism of liver tissue using two-photon flim," Biomed. Opt. Express **11**, 4458–4470 (2020).
45. D. B. Zorov, M. Juhaszova, and S. J. Sollott, "Mitochondrial reactive oxygen species (ros) and ros-induced ros release," Physiol. Rev. **94**, 909–950 (2014).
46. E. Panieri and M. Santoro, "Ros homeostasis and metabolism: a dangerous liason in cancer cells," Cell Death Dis. **7**, e2253 (2016).

Biomedical Optics EXPRESS

47. J. Hua, Z. Xiong, J. Lowey, E. Suh, and E. R. Dougherty, "Optimal number of features as a function of sample size for various classification rules," Bioinformatics **21**, 1509–1515 (2005).
48. J. Neuberger and O. Cain, "The need for alternatives to liver biopsies: non-invasive analytics and diagnostics," HMER **13**, 59–69 (2021).
49. J. Neuberger, J. Patel, H. Caldwell, S. Davies, V. Hebditch, C. Hollywood, S. Hubscher, S. Karkhanis, W. Lester, N. Roslund, R. West, J. I. Wyatt, and M. Heydtmann, "Guidelines on the use of liver biopsy in clinical practice from the British Society of Gastroenterology, The Royal College of Radiologists and the Royal College of Pathology," Gut **69**, 1382–1403 (2020).
50. A. Forner, R. Vilana, C. Ayuso, L. Bianchi, M. Solé, J. R. Ayuso, L. Boix, M. Sala, M. Varela, J. M. Llovet, C. Brú, and J. Bruix, "Diagnosis of hepatic nodules 20 mm or smaller in cirrhosis: prospective validation of the noninvasive diagnostic criteria for hepatocellular carcinoma," Hepatology **47**, 97–104 (2008).